

4-Year COBE¹ DMR Cosmic Microwave Background Observations: Maps and Basic Results

C. L. Bennett^{2,3}, A. Banday⁴, K. M. Górski⁴, G. Hinshaw⁴, P. Jackson⁴, P. Keegstra⁴, A. Kogut⁴,
G. F. Smoot⁵ D. T. Wilkinson⁶ & E. L. Wright⁷

ABSTRACT

The cosmic microwave background radiation provides unique constraints on cosmological models. In this *Letter* we present a summary of the spatial properties of the cosmic microwave background radiation based on the full 4 years of *COBE* DMR observations, as detailed in a set of companion *Letters*. The anisotropy is consistent with a scale-invariant power law model and Gaussian statistics. With full use of the multi-frequency 4-year DMR data, including our estimate of the effects of Galactic emission, we find a power-law spectral index of $n = 1.2 \pm 0.3$ and a quadrupole normalization $Q_{rms-PS} = 15.3^{+3.8}_{-2.8} \mu\text{K}$. For $n = 1$ the best-fit normalization is $Q_{rms-PS}|_{n=1} = 18 \pm 1.6 \mu\text{K}$. These values are consistent with both our previous 1-year and 2-year results. The results include use of the $\ell = 2$ quadrupole term; exclusion of this term gives consistent results, but with larger uncertainties. The 4-year sky maps, presented in this *Letter*, portray an accurate overall visual impression of the anisotropy since the signal-to-noise ratio is ~ 2 per 10° sky map patch. The improved signal-to-noise ratio of the 4-year maps also allows for improvements in Galactic modeling and limits on non-Gaussian statistics.

Subject headings: cosmic microwave background – cosmology: observations

¹NASA/GSFC is responsible for the design, development, and operations of the *COBE*. Scientific guidance is provided by the *COBE* Science Working Group. GSFC is also responsible for the development of the analysis software and the delivery of the mission data sets.

²Code 685, Laboratory for Astronomy & Solar Physics, Goddard Space Flight Center, Greenbelt, MD 20771.

³e-mail address: bennett@stars.gsfc.nasa.gov

⁴Hughes STX Corporation, Code 685, Laboratory for Astronomy & Solar Physics, Goddard Space Flight Center, Greenbelt, MD 20771.

⁵LBL and UC Berkeley, Berkeley, CA 94720.

⁶Physics Dept., Jadwin Hall, Princeton University, Princeton, NJ 08544-1001.

⁷UCLA Astronomy, P.O. Box 951562, Los Angeles, CA 90095-1562.

1. INTRODUCTION

NASA's *COBE* Differential Microwave Radiometers (DMR) experiment (Smoot et al. 1990, Bennett et al. 1991) discovered cosmic microwave background (CMB) anisotropies based on its first year of data (Smoot et al. 1992, Bennett et al. 1992, Wright et al. 1992). The CMB temperature fluctuations were measured at an angular resolution of 7° at frequencies of 31.5, 53, and 90 GHz. These results were supported by a detailed examination of the DMR calibration and its uncertainties (Bennett et al. 1991) and a detailed treatment of the upper limits on residual systematic errors (Kogut et al. 1992). Bennett et al. (1992) showed that spatially correlated Galactic free-free and dust emission could not mimic the frequency spectrum nor the spatial distribution of the observed fluctuations. Bennett et al. (1993) also showed that the pattern of fluctuations does not spatially correlate with known extragalactic source distributions. Confirmation of the *COBE* results was attained by the positive cross-correlation between the *COBE* data and data from balloon-borne observations at a shorter wavelength (Ganga et al. 1993). Bennett et al. (1994) reported the results from analyses of two years of DMR data. The results from the two year data were consistent with those from the first year alone. In this *Letter* we summarize the results and cosmological implications obtained from the full *COBE* DMR 4-year data, and provide references to further detailed reports of our analyses.

Primordial gravitational potential fluctuations were predicted to have an equal *rms* amplitude on all scales (Peebles & Yu 1970, Harrison 1970, Zeldovich 1972). This corresponds to a matter fluctuation power-law spectrum, $P(k) \propto k^n$, where k is the comoving wavenumber, with $n = 1$. Such a spectrum is also a natural consequence of inflationary models. If the effects of a standard cold dark matter model are included, *COBE* DMR should find $n_{eff} \approx 1.1$ for a Peebles-Harrison-Zeldovich $n = 1$ universe. The power spectrum of the *COBE* DMR data is consistent with this.

A cosmological model does not predict the exact CMB temperature that would be observed in our sky, but rather predicts a statistical distribution of anisotropy parameters, such as spherical harmonic amplitudes. In the context of such models, the true CMB temperature observed in our sky is only a single realization from a statistical distribution. Thus, in addition to experimental uncertainties, we account for *cosmic variance* uncertainties in our analyses of the DMR maps. For a spherical harmonic temperature expansion $T(\theta, \phi) = \sum_{\ell m} a_{\ell m} Y_{\ell m}(\theta, \phi)$, cosmic variance is approximately expressed as $\sigma(C_\ell)/C_\ell \approx \sqrt{2/(2\ell + 1)}$ where $C_\ell = \langle |a_{\ell m}|^2 \rangle$. Cosmic variance exists independent of the quality of the experiment. The power spectrum from the 4-year DMR map is cosmic variance limited for $\ell \lesssim 20$.

This *Letter* includes a summary of the key results of a set of detailed DMR 4-year analysis papers (Banday et al. 1996a, 1996b; Gorski et al. 1996; Kogut et al. 1996a, 1996b, 1996c; Hinshaw et al. 1996a, 1996b; Wright et al. 1996).

2. OBSERVATIONS

DMR consists of 6 differential microwave radiometers: 2 nearly independent channels, labeled A and B, at frequencies 31.5, 53, and 90 GHz (wavelength 9.5, 5.7, and 3.3 mm). Each radiometer measures the difference in power between two 7° fields of view separated by 60° , 30° to either side of the spacecraft spin axis (Smoot et al. 1990). *COBE* was launched from Vandenberg Air Force Base on 18 November 1989 into a 900 km, 99° inclination circular orbit, which precesses to follow the terminator. Attitude control keeps the spacecraft pointed away from the Earth and nearly perpendicular to the Sun so that solar radiation never directly illuminates the aperture plane. The combined motions of the spacecraft spin (75 s period), orbit (103 m period), and orbital precession ($\sim 1^\circ$ per day) allow each sky position to be compared to all others through a highly redundant set of temperature difference measurements spaced 60° apart. The on-board processor integrates the differential signal from each channel for 0.5 s, and records the digitized differences for daily playback to a ground station.

Ground data analysis consists of calibration, extensive systematic error analyses, and conversion of time-ordered-data to sky maps (Kogut et al. 1996a). The DMR time-ordered-data include systematic effects such as emission from the Earth and Moon, the instrument’s response to thermal changes, and the instrument’s response to the Earth’s magnetic field. The largest detected effects do not contribute significantly to the DMR maps: they are either on time scales long compared to the spacecraft spin sampling (e.g. thermal gain drifts) or have time dependence inconsistent with emission fixed on the celestial sphere (e.g. magnetic effects). Detected and potential systematic effects were quantitatively analyzed in detail by Kogut et al. (1996a). Data with the worst systematic contamination (lunar emission, terrestrial emission, and thermal gain changes) were not used in the map making process and constitute less than 10% of the data in the 53 and 90 GHz channels. The remaining data were corrected using models of each effect. The data editing and correction parameters were conservatively chosen so that systematic artifacts, after correction, are less than $6 \mu\text{K}$ (95% confidence upper limit) in the final DMR map in the worst channel. This is significantly less than the levels of the noise and celestial signals.

We subtract a dipole (with Cartesian components $[X,Y,Z] = [-0.2173, -2.2451, +2.4853]$ mK thermodynamic temperature in Galactic coordinates) from the time-ordered differential data prior to forming the 4-year sky maps to reduce spatial gradients within a single pixel. A small residual dipole remains in the maps from a combination of CMB and Galactic emission. Fig. 1 shows the full sky maps at each frequency, after averaging the A and B channels, removing the CMB dipole, and smoothing to 10° effective resolution. Table 1 shows the instrument noise per half-second observation. The mean signal-to-noise ratios in the 10° smoothed maps are ~ 0.5 , 1.5, and 1.0 for 31, 53, and 90 GHz, respectively. For a multi-frequency co-added map the signal-to-noise ratio is ~ 2 . This signal-to-noise level is adequate to portray an accurate overall visual impression of the anisotropy. This is illustrated in Fig. 2, where simulated data are shown in combination with the noise appropriate to 1-, 2-, and 4-years of DMR 53 GHz observations.

Given the sensitivity of the 4-year DMR maps we have chosen to extend the cut made in our previous analyses to exclude additional Galactic emission. Along with the previous $|b| < 20^\circ$ exclusion zone, we use the *COBE* DIRBE 140 μm map as a guide to cut additional Galactic emission features. The full sky DMR maps contain 6144 pixels. An optimum Galactic cut maximizes the number of remaining pixels while minimizing the Galactic contamination. Fig. 3 shows the residual Galactic signal as a function of the number of usable pixels after a cut is applied based on the 140 μm DIRBE intensity. Our cut leaves 3881 pixels (in Galactic pixelization) while eliminating the strongest $|b| > 20^\circ$ Galactic emission. Moderate changes to this custom cut will cause derived CMB parameters to change somewhat, but this is consistent with the data sampling differences of real CMB anisotropy features and not necessarily Galactic contamination. Likewise, derived CMB parameters also vary by the expected amount when the maps are made in ecliptic rather than Galactic coordinates since about 1/2 of the noise is re-binned.

Kogut et al. (1996b) examine the Galactic contamination of the surviving high Galactic latitude regions of the DMR maps after the ‘custom cut’ (described above) is applied. No significant cross-correlation is found between the DMR maps and either the 408 MHz synchrotron map or the synchrotron map derived from a magnetic field model (Bennett et al. 1992). This places an upper limit $T_{\text{synch}} < 11 \mu\text{K}$ (95% confidence) on synchrotron emission at 31 GHz.

A significant correlation is found between the DMR maps and the dust-dominated DIRBE 140 μm map, with frequency dependence consistent with a superposition of dust and free-free emission. This corresponds to a 7° rms free-free emission component of $7.1 \pm 1.7 \mu\text{K}$ at 53 GHz and a dust component of $2.7 \pm 1.3 \mu\text{K}$ at 53 GHz. Since this emission is uncorrelated with CMB anisotropies it constitutes $< 10\%$ of the CMB power. The amplitude of the correlated free-free component at 53 GHz agrees with a noisier estimate of free-free emission derived from a linear combination of DMR data which includes *all* emission with free-free spectral dependence. The combined dust and free-free emission contribute $10 \pm 4 \mu\text{K}$ rms at both 53 and 90 GHz, well below the 30 μK cosmic signal. These Galactic signal analyses are consistent with the fact that the fitted cosmological parameters are nearly unaffected by removal of modeled Galactic signals (Górski et al. 1996, Hinshaw et al. 1996), with the notable exception of the quadrupole, which has significant Galactic contamination (Kogut et al. 1996b). A search by Banday et al. (1996a) finds no evidence for significant extragalactic contamination of the DMR maps.

3. INTERPRETATION

Monopole $\ell = 0$: Despite the fact that the DMR is a differential instrument, the known motion of the *COBE* spacecraft about the Earth and the motion of the Earth about the Solar System barycenter allows a determination of the CMB monopole temperature from the DMR data. The CMB at millimeter wavelengths is well described by a blackbody spectrum (Mather et

al. 1994, Fixsen et al. 1996). The Doppler effect from the combined spacecraft and Earth orbital motions creates a dipole signal $T(\theta) = T_0[1 + \beta \cos(\theta) + O(\beta^2)]$, where $\beta = v/c$ and θ is the angle relative to the time-dependent velocity vector. The satellite and Earth orbital motions are well known and change in a regular fashion, allowing their Doppler signal to be separated from fixed celestial signals. We fit the time-ordered data to the Doppler dipole and recover a value for the CMB monopole temperature, $T_0 = 2.725 \pm 0.020$ K (Kogut et al. 1996a).

Dipole $\ell = 1$: The CMB anisotropy is dominated by a dipole term usually attributed to the motion of the Solar System with respect to the CMB rest frame, as seen in Fig. 4. A precise determination of the dipole must account for Galactic emission and the aliasing of power from higher multipole orders once pixels near the Galactic plane are discarded. We account for Galactic emission using a linear combination of the DMR maps or by cross-correlating the DMR maps with template sky maps dominated by Galactic emission (Kogut et al. 1996b). We fit the high-latitude portion of the sky for a dipole with a CMB frequency spectrum using a pixel-based likelihood analysis (Hinshaw et al. 1996a). Accounting for the smoothing by the DMR beam and map pixelization, the CMB dipole has amplitude 3.353 ± 0.024 mK toward Galactic coordinates $(l, b) = (264^\circ.26 \pm 0^\circ.33, 48^\circ.22 \pm 0^\circ.13)$, or equatorial coordinates $(\alpha, \delta) = (11^{\text{h}}12^{\text{m}}2 \pm 0^{\text{m}}8, -7^\circ.06 \pm 0^\circ.16)$ epoch J2000.

Quadrupole $\ell = 2$: On the largest angular scales (e.g., quadrupole), Galactic emission is comparable in amplitude to the anisotropy in the CMB. We use a likelihood analysis to fit the high-latitude portion of the DMR maps for Galactic emission traced by synchrotron- and dust-dominated surveys and a quadrupole anisotropy with a thermodynamic frequency spectrum (Kogut et al. 1996b, Hinshaw et al. 1996a). After correcting for the positive bias from instrument noise and aliasing, the CMB quadrupole amplitude observed at high latitude is $Q_{rms} = 10.7 \pm 3.6 \pm 7.1$ μK , where the quoted errors reflect the 68% confidence uncertainties from random statistical errors and Galactic modeling errors, respectively. The observed quadrupole amplitude, Q_{rms} , has a lower value than the quadrupole expected from a fit to the entire power spectrum, Q_{rms-PS} , but whether this is a chance result of cosmic variance or reflects the cosmology of the universe can not be determined from *COBE* data. The 68% confidence interval for the quadrupole amplitude, $6 \mu\text{K} \leq Q_{rms} \leq 17 \mu\text{K}$, is consistent with the quadrupole normalization of the full power spectrum power-law fit (discussed below): $Q_{rms-PS} = 15.3^{+3.8}_{-2.8}$ μK .

Power spectrum $\ell \geq 2$: The simplest probe of the angular power spectrum of the anisotropy is its Legendre transform, the 2-point correlation function. The 2-point correlation function of the 4-year maps is analyzed by Hinshaw et al. (1996b), where it is shown that the 2-point data are consistent from channel to channel and frequency to frequency. The data are robust with respect to the angular power spectrum. As in Bennett et al. (1994), we use a Monte Carlo-based Gaussian likelihood analysis to infer the most-likely quadrupole normalization for a scale-invariant ($n = 1$) power-law spectrum. The results are summarized in Table 2 where we also include the results of 3 additional, independent power spectrum analyses, discussed below. The normalization inferred from the 2-point function is now in better agreement with other determinations than was the case

with the 2-year data. The change is due to data selection: with the 2-year data, we only analyzed the 53×90 GHz cross-correlation function; with the 4-year data we have analyzed many more data combinations, including the auto-correlation of a co-added, multi-frequency map. This latter combination is more comparable to the data analyzed by other methods, and the 2-point analysis yields consistent results in that case. The combined 31, 53 and 90 GHz CMB rms is $29 \pm 1 \mu\text{K}$ in the 10° smoothed map (Banday et al. 1996b), consistent with the level determined by the 2-point results.

It is also possible to analyze the power spectrum directly in terms of spherical harmonics. However, there is considerable subtlety in this because the removal of the Galactic plane renders the harmonics non-orthonormal, producing strong correlations among the fitted amplitudes. Wright et al. (1996) has solved for an angular power spectrum by modifying and applying the technique described by Peebles (1973) and Hauser & Peebles (1973) for data on the cut sphere. They compute a Gaussian likelihood on these data and calibrate their results with Monte Carlo simulations. Górski et al. (1996) explicitly construct orthonormal functions on the cut sphere and decompose the anisotropy data with respect to these modes. They form and evaluate an exact Gaussian likelihood directly in terms of this mode decomposition. The results of these analyses are summarized in Table 2. Further details, including results from other data combinations are given in the respective papers.

Hinshaw et al. (1996a) evaluate a Gaussian likelihood directly in terms of a full pixel-pixel covariance matrix, a technique applied to the 2-year data by Tegmark & Bunn (1995). The results of the power-law spectrum fits are summarized in Table 2. Hinshaw et al. (1996a) also analyze the quadrupole anisotropy separately from the higher-order modes, to complement the analysis of Kogut et al. (1996b). They compute a likelihood for the quadrupole mode C_2 , nearly independent of higher-order power, and show that it peaks between 6 and 10 μK , depending on Galactic model, but that its distribution is so wide that it is easily consistent with $15.3_{-2.8}^{+3.8} \mu\text{K}$, the value derived using the full power spectrum.

Tests for Gaussian Statistics: It is important to determine whether the primordial fluctuations are Gaussian. The probability distribution of temperature residuals should be close to Gaussian if the sky variance is Gaussian and the receiver noise is Gaussian. The receiver noise varies somewhat from pixel to pixel because the observation times are not all the same, but when this is taken into account the data appear Gaussian (Smoot et al. 1994). There is no evidence for an excess of large deviations, as would be expected if there were an unknown population of point sources. A search for point sources in the 2-year maps was negative (Kogut et al. 1994). Given the large beam of the instrument and the variance of both cosmic signals and receiver noise, it is still possible for interesting signals to be hidden in the data.

Kogut et al. (1996c) compare the 4-year DMR maps to Monte Carlo simulations of Gaussian power-law CMB anisotropy. The 3-point correlation function, the 2-point correlation of temperature extrema, and the topological genus are all in excellent agreement with the hypothesis

that the CMB anisotropy on angular scales of 7° or larger represents a random-phase Gaussian field. A likelihood comparison of the DMR maps against non-Gaussian χ^2_N toy models tests the alternate hypothesis that the CMB is a random realization of a field whose spherical harmonic coefficients $a_{\ell m}$ are drawn from a χ^2 distribution with N degrees of freedom. Not only do Gaussian power-law models provide an adequate description of the large-scale CMB anisotropy, but non-Gaussian models with $1 < N < 60$ are five times less likely to describe the true statistical distribution than the exact Gaussian model.

4. SUMMARY OF 4-YEAR *COBE* DMR CMB MEASUREMENTS

(1) The full 4-year set of *COBE* DMR observations is analyzed and full sky maps are presented. The typical signal-to-noise ratio in a 10° smoothed map is ~ 2 in the frequency-averaged map, enough to provide a visual impression of the anisotropy.

(2) We derive a CMB monopole temperature from DMR (despite its being a differential instrument) of $T_0 = 2.725 \pm 0.020$ K (Kogut et al. 1996a). This is in excellent agreement with the *COBE* FIRAS precision measurement of the spectrum of the CMB, $T_0 = 2.728 \pm 0.002$ K (Fixsen et al. 1996).

(3) The CMB dipole from DMR has amplitude 3.353 ± 0.024 mK toward Galactic coordinates $(l, b) = (264^\circ.26 \pm 0^\circ.33, 48^\circ.22 \pm 0^\circ.13)$, or equatorial coordinates $(\alpha, \delta) = (11^{\text{h}}12^{\text{m}}2 \pm 0^{\text{m}}8, -7^\circ.06 \pm 0^\circ.16)$ epoch J2000. This is consistent with the dipole amplitude and direction derived by *COBE* FIRAS (Fixsen et al. 1996).

(4) The 95% confidence interval for the observed $\ell = 2$ quadrupole amplitude is $4 \mu\text{K} \leq Q_{rms} \leq 28 \mu\text{K}$. This is consistent with the value predicted by a power-law fit to the power spectrum: $Q_{rms-PS} = 15.3^{+3.8}_{-2.8} \mu\text{K}$ (Kogut et al. 1996b; Hinshaw et al. 1996a).

(5) The power spectrum of large angular scale CMB measurements are consistent with an $n = 1$ power-law (Górski et al. 1996, Hinshaw et al. 1996a, Wright et al. 1996). If the effects of a standard cold dark matter model are included, *COBE* DMR should find $n_{eff} \approx 1.1$ for a $n = 1$ universe.) With full use of the multi-frequency 4-year DMR data, including our estimate of the effects of Galactic emission, we find a power-law spectral index of $n = 1.2 \pm 0.3$ and a quadrupole normalization $Q_{rms-PS} = 15.3^{+3.8}_{-2.8} \mu\text{K}$. For $n = 1$ the best-fit normalization is $Q_{rms-PS}|_{n=1} = 18 \pm 1.6 \mu\text{K}$. Differences in the derived values of Q and n between various analyses of DMR data are much more dependent on the detailed data selection effects than on the analysis technique.

(6) The DMR anisotropy data are consistent with Gaussian statistics. Statistical tests prefer Gaussian over other toy statistical models by a factor of ~ 5 (Kogut et al. 1996c).

The DMR time-ordered data, map data, and ancillary data sets (including our custom

Galactic cut) are publicly available through the National Space Science Data Center (NSSDC) at http://www.gsfc.nasa.gov/astro/cobe/cobe_home.html. We gratefully acknowledge the *COBE* support provided by the NASA Office of Space Sciences (OSS). We also acknowledge the contributions of J. Aymon, V. Kumar, R. Kummerer, C. Lineweaver, J. Santana, and L. Tenorio.

REFERENCES

- Banday, A. et al. 1996a, *ApJ*, to be submitted
- Banday, A. et al. 1996b, *ApJ*, submitted
- Bennett, C. L., et al. 1994, *ApJ*, 436, 423
- Bennett, C. L., et al. 1993, *ApJ*, 414, L77
- Bennett, C. L., et al. 1992, *ApJ*, 396, L7
- Bennett, C. L., et al. 1991, *ApJ*, 391, 466
- Fixsen, D. J., et al. 1996, *ApJ*, submitted
- Ganga, K., et al. 1993, *ApJ*, 410, L57
- Górski et al., K. M. 1996, *ApJ*, submitted
- Harrison, E. R. 1970, *Phys. Rev. D*, 1, 2726
- Hauser, M. G. & Peebles, P. J. E. 1973, *ApJ*, 185, 757
- Hinshaw, G., et al. 1996a, *ApJ Letters*, submitted
- Hinshaw, G., et al. 1996b, *ApJ Letters*, submitted
- Kogut, A., et al. 1992, *ApJ*, 401, 1
- Kogut, A., Banday, A. J., Bennett, C. L., Hinshaw, G., Loewenstein, K., Lubin, P., Smoot, G. F., & Wright, E. L. 1994, *ApJ*, 433, 435
- Kogut, A., et al. 1996a, *ApJ*, submitted
- Kogut, A., et al. 1996b, *ApJ*, submitted
- Kogut, A., et al. 1996c, *ApJ*, submitted
- Mather, J. C., et al. 1994, *ApJ*, 420, 439
- Peebles, P. J. E. 1973, *ApJ*, 185, 413

Peebles, P. J. E. & Yu, J. T. 1970, ApJ, 162, 815

Smoot, G. F., Tenorio, L., Banday, A.J., Kogut, A., Wright, E.L., Hinshaw, G., & Bennett, C.L. 1994, ApJ, 437, 1

Smoot, G. F., et al. 1992, ApJ, 396, L1

Smoot, G.F., et al. 1990, ApJ, 360, 685

Tegmark, M. & Bunn, E. F. 1995, ApJ, 455, 1

Wright, E. L., et al. 1996, ApJ Letters, submitted

Wright, E. L., et al. 1992, ApJ, 396, L13

Zeldovich, Ya B. 1972, MNRAS, 160, 1

FIGURE CAPTIONS

Figure 1: [color plate] Full sky Mollweide projections of the 31, 53, and 90 GHz 4-year maps formed by averaging the A and B channels at each frequency. After the mean offset and the dipole are removed, the bright (red) emission from the Galaxy dominates the central band of the maps.

Figure 2: [color plate] (*top left*) Full sky simulation of an anisotropy map smoothed to 10° resolution with an $n = 1$ Peebles-Harrison-Zeldovich power spectrum with $Q_{rms-PS} = 18 \mu\text{K}$. DMR instrument noise is added to the sky simulation corresponding to: (*top right*) 1-year; (*bottom right*) 2-years; (*bottom left*) 4-years of observations. Note the good visual agreement between the ‘true’ sky on the top left and the 4-year simulated DMR result on the bottom left.

Figure 3: The estimated residual Galactic signal at 53 GHz as a function of the number of surviving map pixels after the application of an intensity cut that is based on the DIRBE $140 \mu\text{m}$ map. The conversion from DIRBE intensity to DMR 53 GHz intensity is from a correlation study (Kogut et al. 1996b). A minimum $|b| < 20^\circ$ cut is always applied, leaving at most 4016 pixels. The arrows indicate the intensity cut that we chose to maximize the remaining number of pixels while minimizing the Galactic contamination. This leaves 3881 map pixels for CMB analysis. A simple $|b| < 30^\circ$ cut produces the peak-to-peak intensity and rms shown by the ‘+’ symbols, and is obviously less efficient than the custom cut.

Figure 4: [color plate] (*top*) Full sky Mollweide projection of the 4-year 53 GHz DMR map, including the dipole. (*middle*) Full sky Mollweide projection of the 4-year 53 GHz DMR map, excluding the dipole. (*bottom*) Full sky Mollweide projection of the 4-year DMR map, excluding the dipole, using data from 31, 53, and 90 GHz with modeled Galactic emission removed, and the Galactic custom cut applied.

Table 1. DMR Instrument Noise in Antenna Temperature

Channel	Noise per 0.5 sec Observation (mK)
31A	58.27
31B	58.35
53A	23.13
53B	27.12
90A	39.10
90B	30.76

Table 2. Summary of DMR 4-Year Power Spectrum Results

Statistic	n^a	Q_{rms-PS}^b (μK)	$Q_{rms-PS n=1}^c$ (μK)
No Galaxy Correction ^d			
2-point function ^e	—	—	$18.6^{+1.4}_{-1.4}$
Orthog. functions ^f	$1.23^{+0.23}_{-0.29}$	$15.3^{+3.9}_{-2.6}$	$18.3^{+1.3}_{-1.2}$
Pixel temps ^g	$1.25^{+0.26}_{-0.29}$	$15.4^{+3.9}_{-2.9}$	$18.4^{+1.4}_{-1.3}$
Hauser-Peebles ^h	$1.30^{+0.30}_{-0.34}$	—	$17.7^{+1.4}_{-1.8}$
DIRBE-Template Galaxy Correction ⁱ			
2-point function ^e	—	—	$17.5^{+1.4}_{-1.4}$
Orthog. functions ^f	$1.21^{+0.24}_{-0.28}$	$15.2^{+3.7}_{-2.6}$	$17.7^{+1.3}_{-1.2}$
Pixel temps ^g	$1.23^{+0.26}_{-0.27}$	$15.2^{+3.6}_{-2.8}$	$17.8^{+1.3}_{-1.3}$
Hauser-Peebles ^h	—	—	—
Internal Combination Galaxy Correction ^j			
2-point function ^e	—	—	$16.7^{+2.0}_{-2.0}$
Orthog. functions ^f	$1.11^{+0.38}_{-0.42}$	$16.3^{+5.2}_{-3.7}$	$17.4^{+1.8}_{-1.7}$
Pixel temps ^g	$1.00^{+0.40}_{-0.43}$	$17.2^{+5.6}_{-4.0}$	$17.2^{+1.9}_{-1.7}$
Hauser-Peebles ^h	$1.62^{+0.44}_{-0.50}$	—	$19.6^{+2.5}_{-2.5}$

^aMode and 68% confidence range of the projection of the 2-dimensional likelihood, $L(Q, n)$, on n

^bMode and 68% confidence range of the projection of the 2-dimensional likelihood, $L(Q, n)$, on Q

^cMode and 68% confidence range of the slice of the 2-dimensional likelihood, $L(Q, n)$, at $n = 1$

^dFormed from the weighted average of all 6 channels

^eHinshaw et al. 1996b

^fGórski et al. 1996

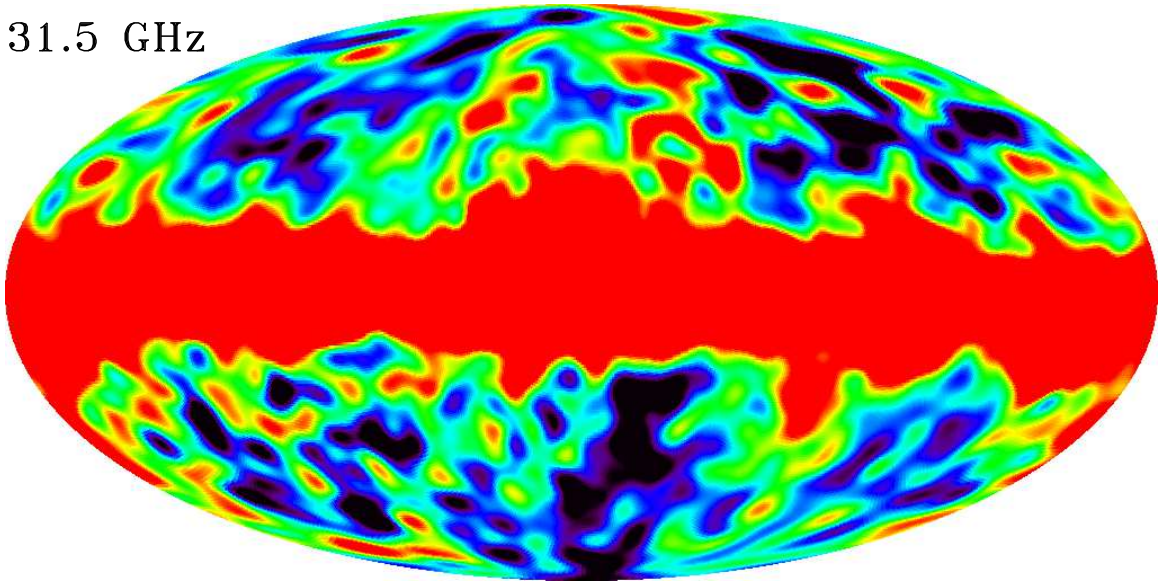
^gHinshaw et al. 1996a

^hWright et al. 1996; in this case data selection differs slightly, as described in the reference

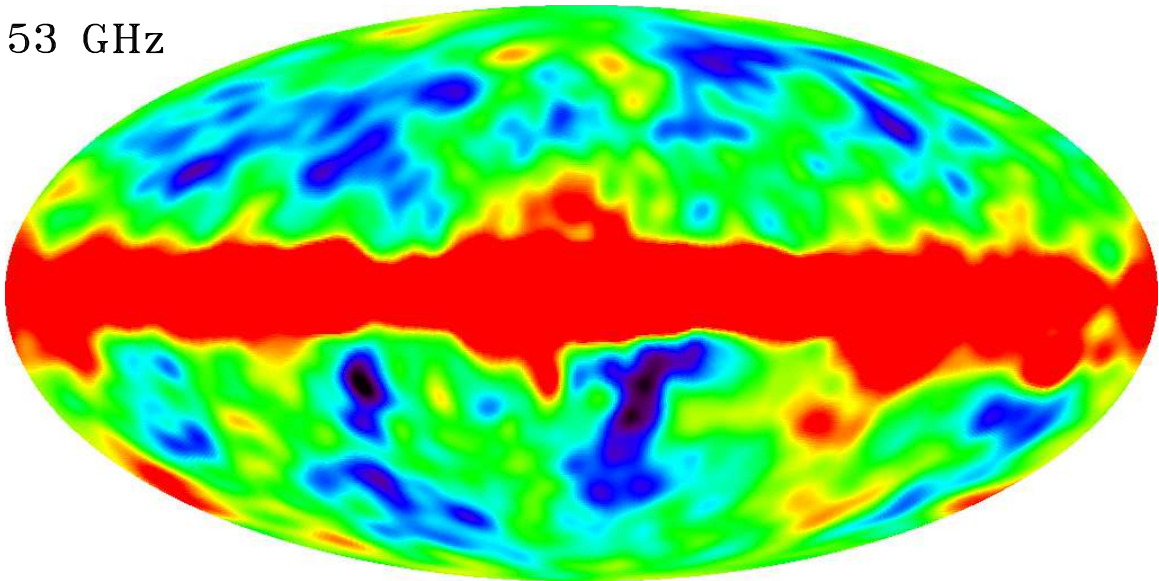
ⁱFormed from the weighted average of all 6 channels with the best-fit Galactic template maps subtracted (Kogut et al. 1996b)

^jFormed from a linear combination of all 6 channel maps that cancels free-free emission (Kogut et al. 1996)

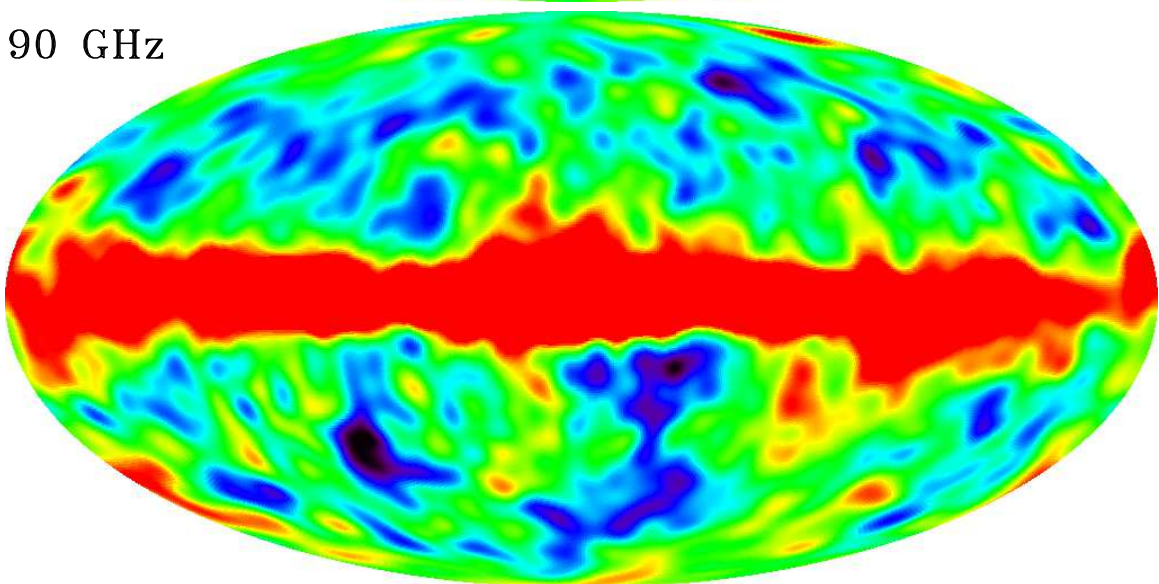
31.5 GHz



53 GHz



90 GHz



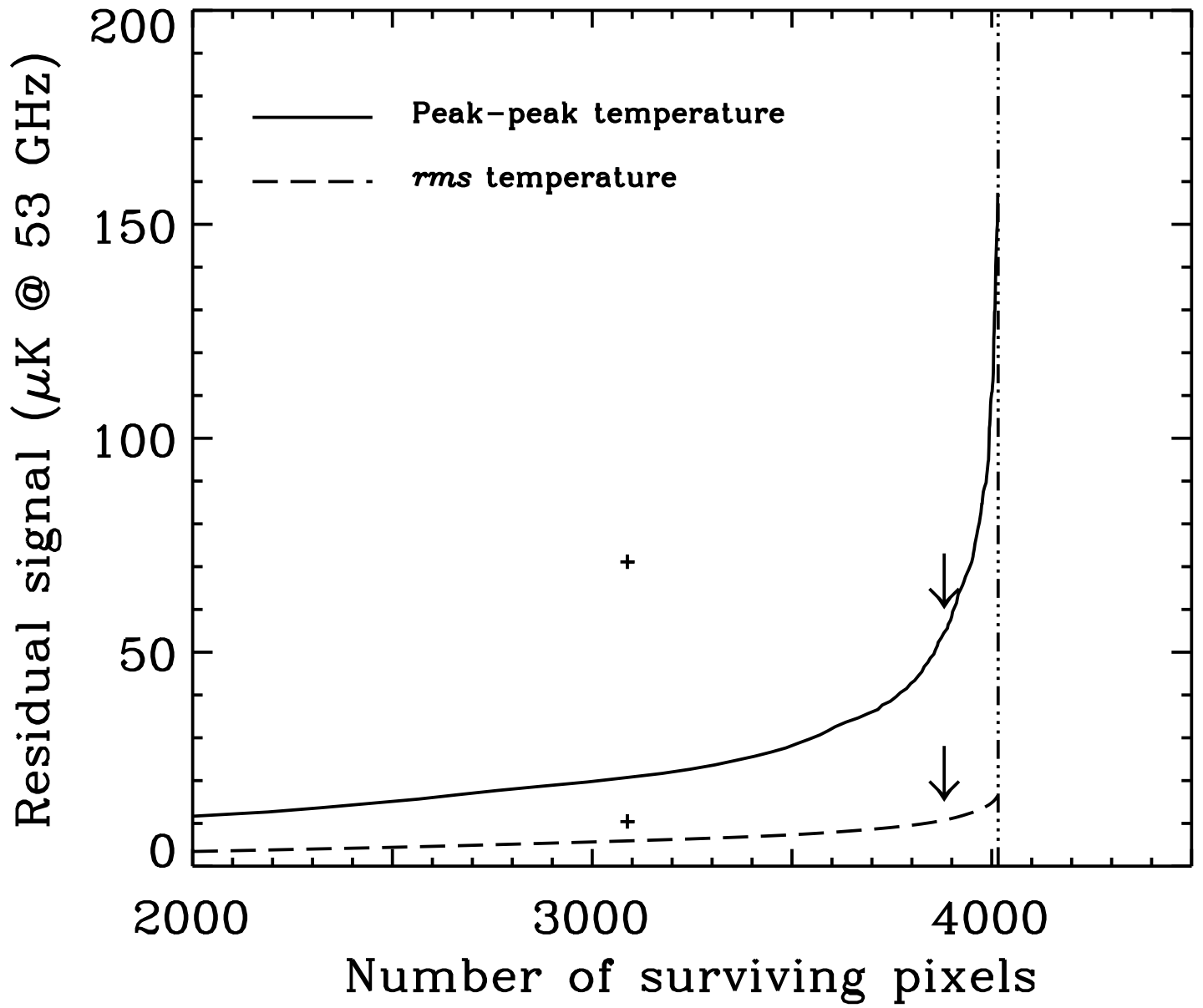
-100 μK  +100 μK

This figure "fig1-1.png" is available in "png" format from:

<http://arxiv.org/ps/astro-ph/9601067v1>

This figure "fig1-2.png" is available in "png" format from:

<http://arxiv.org/ps/astro-ph/9601067v1>



This figure "fig1-3.png" is available in "png" format from:

<http://arxiv.org/ps/astro-ph/9601067v1>